



IJPPR

INTERNATIONAL JOURNAL OF PHARMACY & PHARMACEUTICAL RESEARCH
An official Publication of Human Journals

ISSN 2349-7203




Human Journals

Research Article


October 2019 Vol.:16, Issue:3

© All rights are reserved by Abdel Boughriet et al.

Hazardous Iron in Contaminated Ground Water (A Special Focus in Central African Republic): Health Risk Assessment and Efficient Ferrous Ions Removal by Activated Brick



IJPPR
INTERNATIONAL JOURNAL OF PHARMACY & PHARMACEUTICAL RESEARCH
An official Publication of Human Journals



ISSN 2349-7203

**Nicole Poumaye^{1,2}, Oscar Allahdin^{1,2}, Michel Wartel²,
Abdel Boughriet^{2*}**

*1. Chaire Unesco « Sur la gestion de l'eau »,
Laboratoire Hydrosociences Lavoisier, Université de
Bangui, Faculté des Sciences, B.P. 908, République
Centrafricaine.*

*2. Université Lille, Laboratoire LASIR (UMR CNRS
8516), Equipe Physico-chimie de l'Environnement. Bât.
C8 2^{ème} étage, 59655 Villeneuve d'Ascq cedex, France.*

Submission: 25 September 2019
Accepted: 30 September 2019
Published: 30 October 2019



HUMAN JOURNALS

www.ijppr.humanjournals.com

Keywords: Brick; Activation; Adsorption; Fe(II); Ground Water; Health risk; Permissible Limit

ABSTRACT

A brick made in Bangui region (Central African republic) was treated with sodium hydroxide and used for continuous removal of Fe(II) ions from aqueous solutions in a packed-bed column. An inlet metal concentration of about 10.5 mg.L⁻¹ and a flow rate of 5 mL.min⁻¹ were investigated in continuous column operations resulting in effluent Fe(II) concentrations varying from 1µg.L⁻¹ to 8µL⁻¹ of Fe(II), which are well below the permissible limit recommended by WHO for drinking water (300µg.L⁻¹). The adsorption performance of the column was successfully predicted using the Thomas model. Three adsorption-desorption cycles were carried out with regeneration efficiencies of about 34% using 1.5mol.L⁻¹ NaCl followed by a 0.01mol.L⁻¹NaOH leaching. Adsorption capacity then decreased from 6.7 mg.g⁻¹ to 2.3 mg.g⁻¹ over three cycles, however, it increased again up to 3.1 mg.g⁻¹ if the column brick was regenerated subsequently with a higher NaOH concentration (0.6mol.L⁻¹). These investigations revealed that alkali brick could be employed as an easily accessible, abundant, and low cost adsorbent for the removal of Fe(II) from ground waters in a simple regenerable continuous-flow system that ought to be implemented in homes belonging to poor/rural people.

1. INTRODUCTION

Iron is an abundant element in the Earth's crust. Ground waters in contact with iron-bearing minerals/rocks can be contaminated by this metal. Under anoxic conditions, this metal occurs in ground waters as ferrous iron in a free dissolved form, Fe^{2+} , and/or as a hydroxide complex $\text{Fe}(\text{OH})^+$. Iron contamination has been reported in different regions around the world, sometimes at elevated levels that have exceeded the permissible limit recommended by the World Health Organization (WHO), *i.e.*: 0.3mg.L^{-1} [1]. Ferrous ion is oxidized progressively by atmospheric oxygen to give ferric iron, $\text{Fe}(\text{III})$, which subsequently precipitates as colloidal iron oxide/hydroxide. Such a precipitation is responsible for domestic issues such as reddish colour, staining of laundry, and solids deposition in the water leading to high turbidity. Furthermore, the atmospheric oxidation of ferrous ions present in ground waters leads to the growth of bacterial micro-organisms. These bacterial proliferations are responsible with time for bad odour and an increase of unpleasant taste [2, 3], and also for serious domestic problems such as clogging of pipes and softeners [4, 5], and even punctures and leakages in the water distribution system [2, 3, 6]. It is further worth noting that accumulation of iron in human body can cause with time health problems (see section 3.1).

Nowadays, safe water is considered as being one of the most basic human necessities for guaranteeing a good human health. Unfortunately, water-treatment technologies used by drinking water supply companies are extremely expensive in terms of maintenance and operational costs for people in developing countries. Thereby, household water treatment are often considered as a more appropriate way to deal with the problem of polluted water in rural and remote regions of developing countries. This has constrained us to develop simple and low-cost effective and environmental friendly methods by carrying out *first* laboratory scale researches and *second* full scale trials in Central African Republic (CAR). Indeed, in this country many ground water resources are polluted naturally with ferrous ions, and this pollution constitutes a great problem in a country with an increasing population and a decline in the accessibility of clean and safe water. By considering the well-known beneficiary effects of iron oxide(s)/hydroxide(s) on the adsorption characteristics toward metal ions when they were deposited onto certain minerals— for instances: silica and $\text{Al}(\text{OH})_2/\text{SiO}_2$ [7-13], aluminosilicate minerals such as zeolites [14, 15], and hydrated magnesium silicate mineral, sepiolite [16]—, our research group had recently used broken/sieved brick (which is composed mostly of sand and clays) as a material support and impregnated it with

ferrihydrite for removing ferrous ion and other heavy metal cations from aqueous solutions [17-21]. Note that the brick used in these research works was made by craftsmen from local soils in Bangui region.

The first objective of the present work had been to assess the potential health risk of soluble iron to Bangui population as a result of Fe(II)-contaminated ground waters ingestion. The second objective had been to develop an adsorption method by using Bangui brick as adsorbent. This brick was previously modified for improving Fe(II)-adsorption performance according to a new synthesis protocol which was elaborated in the aim to be easily carried out by no-scientists and African rural people. The synthesis was achieved in one stage: a simple reaction between Bangui brick (broken and seized into small pellets with sizes of about 0.7-1.0 mm) and sodium hydroxide (provided from local soap factories) for 6 days at a temperature of 90°C. The synthesized material was characterized by using X-ray diffraction (XRD) and Environmental Scanning Electron Microscopy (ESEM). The ability of the synthesized compound to better absorb ferrous ions was tested in fixed-bed columns and recovered effluent solutions were analyzed by ICP-AES spectroscopy. In order to avoid harmful effects of this metal on human health through ground waters used in CAR, the feasibility of NaOH-treated brick to operate efficiently as adsorbent below the permissible limit prescribed by WHO was examined and discussed.

2. MATERIALS AND METHODS

2.1. Adsorbents preparation

The raw brick used in this study came from Bangui region in Central African Republic. The mineralogy of this brick was previously determined by means of X-ray diffraction (XRD) and chemical analyses [22]: 60-65 wt % quartz (SiO_2) and 20-25 wt % metakaolinite ($2\text{SiO}_2 \cdot \text{Al}_2\text{O}_3$); and to a lesser extent: 4-5 wt % illite; ≤ 4 wt % iron oxides / hydroxides; and ≤ 3 wt % feldspar + mica + biotite. Before use as an adsorbent, several physical / chemical treatments were carried out on the brick. First, it was broken into grains and sieved with sizes ranging from 0.7 to 1.0 mm. Second, brick pellets were treated in our laboratory under the following alkali conditions: : 10 g of Bangui brick reacted in 40 mL of a diluted NaOH solution ($0.6 \text{ mol} \cdot \text{L}^{-1}$) at room temperature for one night under slow shaking at a speed of 120 rpm. This procedure was afterwards followed by a fixed-temperature increase of the mixture at 90°C for a constant reaction time of six days. The recovered grains were afterwards rinsed

several times with Milli-Q water and dried at 90°C for 24 hours, leading to an alkali-brick material called “AB” in this article.

2.2. Chemicals

All chemicals employed in the experiments were analytical grades. Sodium hydroxide and $\text{FeCl}_2 \cdot 4\text{H}_2\text{O}$ were supplied by DISLAB (France).

2.3. ICP-AES analyses

Effluent solutions recovered from fixed-bed columns were analyzed for iron(II) contents using ICP-AES (Inductively Coupled Plasma – Atomic Emission Spectroscopy; model Varian Pro Axial View).

2.4. X-ray diffraction study

XRD patterns were conducted at room temperature in a Bruker D8 Advance diffractometer using Ni-filtered $\text{CuK}\alpha$ radiation (40kV, 40 mA). Samples were scanned with a step size of 0.02° and a counting time of 0.5 sec per step.

2.5. Electron Microscopy analysis

Micrographies of representative specimens of alkali brick were recorded by using an environmental scanning electron microscope (ESEM, Quanta 200 FEI).

2.6. Fixed-bed column experiments

Continuous flow adsorption experiments were conducted in a fixed-bed glass column with an inner diameter of 10 mm, a height of 18 cm, and a 160-250 μm porosity sintered-pyrex disk at its bottom in order to prevent any loss of material. A bed depth of 10.2 cm (10.1 g) was investigated at a constant flow rate of 5 mL/min. Before being used in the experiments, at least 500 mL of Milli-Q water were passed through the column. The schematic diagram of the fixed-bed column reactor used is illustrated in reference 18. Milli-Q water spiked with about $10.5 \text{ mg}\cdot\text{L}^{-1}$ of Fe(II) was used for column tests because the Fe(II) concentration in the contaminated ground waters was usually $< 11 \text{ mg}\cdot\text{L}^{-1}$. The $\text{Fe}(\text{Cl})_2 \cdot 4\text{H}_2\text{O}$ salt was employed for Fe(II) solutions preparation. The influent pH ranged from 4.9 to 5.0. At the iron(II) concentration used ($1.79 \times 10^{-4} \text{ mol}\cdot\text{L}^{-1}$), Fe^{2+} ions remained at oxidation state II under our

physicochemical (O_2 , natural potential Eh and pH) conditions, according to $p_e - pH$ diagrams for iron-water system [23].

Fe^{2+} ions solution was pumped through the column at a desired flow rate by means of a peristaltic pump (LaboModerne France Type KD1170) in an up-flow mode. During the column experiment, the effluent pH was measured continuously by means of a pH meter which was connected to a computer; and effluent samples exiting the upper of the column were collected at different time intervals and analyzed for metal contents using ICP-AES (Inductively Coupled Plasma - Atomic Emission Spectroscopy; model Varian Pro Axial View). Flow to the column continued until the effluent metal concentration at time t (C_t) reached the influent metal concentration (C_0): $C_t/C_0 \approx 0.99$. Performance of the packed bed was described in the present work using the concept of the breakthrough curve. Breakthrough profiles yielded two important times: (i) the breakthrough time, noted t_b , when $C_t = 0.05C_0$; and (ii) the exhaustion time, noted $t_{exh.}$, when $C_t = 0.95C_0$.

3. RESULTS

3.1. Potential health risk due to ground-water ingestion in Bangui region

Previous studies revealed that barely 30% of households in Bangui region accessed potable treated water. And among the remaining 70% of the households, many of them still used unprotected shallow wells in which microbial contamination can further occur in addition to that of soluble iron.

Some of these water sources were deemed unsafe mostly due to elevated levels of soluble iron, and often with values found to be much above the permissible limit recommended by the WHO, *i.e.*: 0.3 mg.L^{-1} . The maximum Fe^{2+} ions concentration in Bangui ground waters can attain up to 10.5 mg.L^{-1} . Such water sources should then pose a threat to human health when consumed untreated.

Several health issues due to high iron content in water were reported in the literature. Briefly, because of elevated levels of iron in human body, different disease symptoms can appear, for instances: (i) the hemotopoesis of bone marrow is injured with damages of hematopoietic stem/progenitor cells (resulting in hemochromatosis); and (ii) toxic substances can then be liberated in human body, deteriorating vital organs, and consequently, being able to cause with time grave diseases such as eye disorders, or even heart and cancer [24-30].

In order to assess the potential health risk associated with iron pollution in Bangui ground waters, we calculated the Estimated Daily Intake (EDI) of iron through water ingestion by Bangui people having drunken strongly Fe - contaminated waters from the equation:

$$EDI = [Fe^{2+}] \cdot D_{aiw} / B_{aw} \quad (1)$$

where $[Fe^{2+}]$ is the concentration of iron(II) (in $\mu\text{g} \cdot \text{L}^{-1}$) in ground water; D_{aiw} is the daily average intake of water (in liter per day, $\text{L} \cdot \text{d}^{-1}$) which is assumed here to be $2 \text{ L} \cdot \text{d}^{-1}$ for adult and $1 \text{ L} \cdot \text{d}^{-1}$ for child according to the United-States Environmental Protection Agency [31]; and B_{aw} represents the body average weights which is assumed here to be 72 kg for adult and 32.7 kg for child [32]. We found a maximum EDI value of $291.7 \mu\text{g} \cdot \text{kg}^{-1} \cdot \text{d}^{-1}$ for adult and $321.1 \mu\text{g} \cdot \text{kg}^{-1} \cdot \text{d}^{-1}$ for child when people drink ground waters containing 10.5 mg of iron per liter. Fortunately, the EDI range $0.29\text{-}0.32 \text{ mg} \cdot \text{kg}^{-1} \cdot \text{d}^{-1}$ calculated for Bangui people drinking the highest levels of Fe-polluted waters, is below that established by USEPA ($0.40\text{-}1.00 \text{ mg} \cdot \text{kg}^{-1} \cdot \text{d}^{-1}$) and as being unlikely to cause immediate adverse effects in healthy persons [30]. Moreover, in order to prevent excessive iron in the human body, it was strongly advised by JECFA a provisional maximum tolerable daily intake of $0.8 \text{ mg} \cdot \text{kg}^{-1} \cdot \text{d}^{-1}$ [30].

As a precaution against storage of excessive iron in the body, Lille University (France) associated with Bangui University (Central African Republic) decided to develop a low-cost/efficient adsorption method for elimination of iron from Bangui ground waters by employing a local brick—which was previously treated with sodium hydroxide—as adsorbent and water spiked with about $10.5 \text{ mg} \cdot \text{L}^{-1}$ of Fe(II) for column tests.

3.2. Crystalline and morphological properties of the brick after NaOH treatment

The X-ray diffractogram of raw-brick powder (Fig. 1'RB') displays mainly the peaks attributed to quartz (SiO_2), and at lower intensities, those of rutile (TiO_2) and illite with the chemical formulae: $(\text{K}, \text{H}_3\text{O})(\text{Al}, \text{Mg}, \text{Fe})_2(\text{Si}, \text{Al})_4\text{O}_{10}[(\text{OH})_2, (\text{H}_2\text{O})]$ [22].

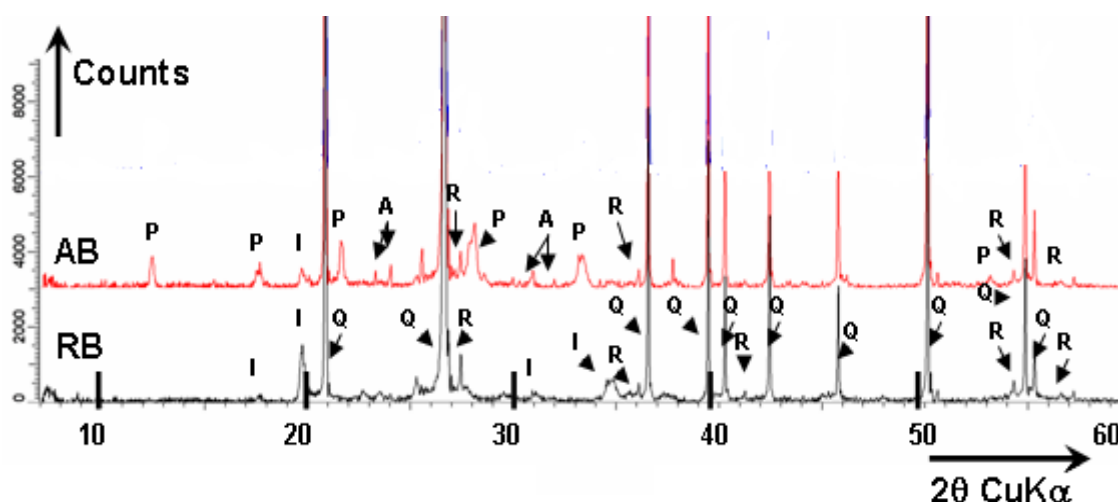


Figure No. 1: XRD patterns of raw brick (*RB*) before and after alkaline treatment. (10 g of raw brick were treated in 40 mL of NaOH solution at 90°C for 6 days in order to form alkali brick called here *AB*). *I*, illite; *Q*, quartz; *R*, rutile; *P*, NaP zeolite; and *A*, NaA zeolite.

The XRD patterns of Bangui-brick powder treated with a 0.6mol.L⁻¹ NaOH solution at 90°C for six days, show five main characteristic peaks attributed to the zeolite LTA at the ‘2θ’ Bragg angles: 7.2°, 12.5°, 16.1°, 30.0° and 30.8° (see Fig. 1’AB’). These reflections correspond to Miller indices (200), (200), (420), (644 and 820) and (822 and 660), respectively [33]. Other peaks ascribed to the zeolite NaP, are detected in the diffractogram of alkali brick (called ‘AB’). The NaP peaks are detected at the following Bragg angles (2θ): 12.5°, 17.7°, 21.7°, 28.1°, and 33.4° that correspond to Miller indices (101), (200 and 002), (211, 112 and 121), (310, 301, and 103) and (213, 312, and 321), respectively [33].

The ESEM image obtained for an alkali-brick sample was compared to that of raw brick (Fig. 2). This latter compound shows mainly quartz crystals associated with aluminosilicate aggregates (clays) with surface roughness and cracks (Fig. 2A).

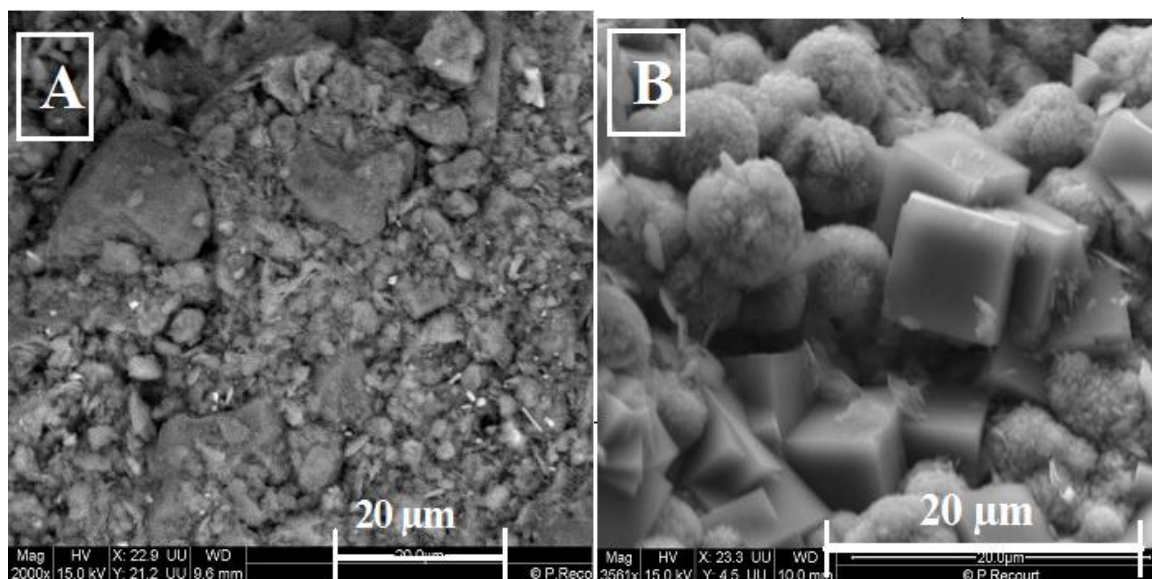


Figure No. 2: ESEM images of raw brick (A); and alkaline brick (B) which was synthesized at 90°C for 6 days (10 g of raw brick treated in 40 mL of a 0.6mol.L⁻¹ NaOH solution).

As for that of NaOH-treated brick, it displays two types of micro-structures (Fig. 2B) in addition to quartz crystals: (i) one with cubic shapes and diameter sizes ranging from 5 to 10 µm; and (ii) the other with spherical shapes and with diameter sizes varying from 3 to 7 µm. Cubic crystals were found to be comparable with those observed previously for the A-type zeolite using the SEM technique [34, 35]. As for spherical shape crystals, they were found to be morphologically similar to those reported in the literature for zeolite NaP [36-39].

3.3. Column capacity modeling

As column capacity yields important information on uptake potential from solutions containing ferrous ions content, it should also provide valuable insights on the future utility of “zeolitized brick” for similar iron(II) removal applications directly in the *field* (in CAR). The column performances were evaluated through the breakthrough curve of the continuous fixed-bed column (Fig. 3).

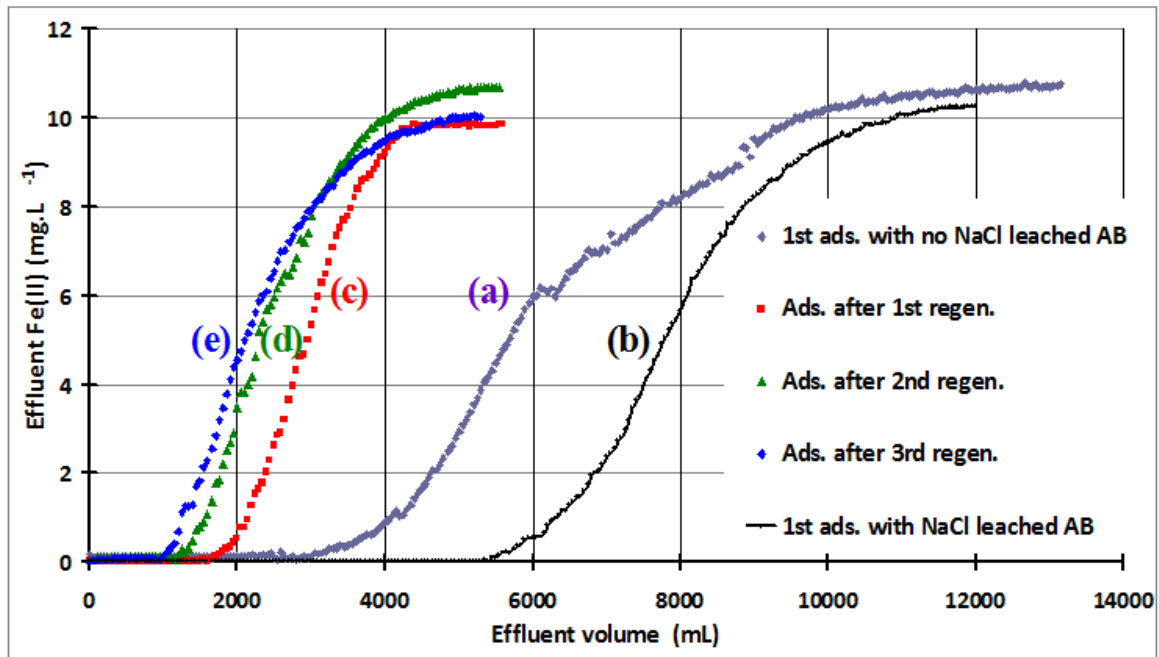


Figure No. 3: Breakthrough curves relative to the removal of Fe²⁺ ions in fixed-bed column by alkali brick before and after column regeneration.

The breakthrough curve corresponding to the removal of Fe²⁺ ions by the alkali brick from a diluted Fe(II) solution (10.7 mg.L⁻¹) is shown in Fig. 3a. A steeper breakthrough curve and higher adsorption performance were obtained when a 1.5mol.L⁻¹ NaCl solution (about 200 mL) was passed through the column before performing Fe(II)-adsorption (see Fig. 3b), indicating a shorter mass transfer zone in the column [40-42]. The shape of the breakthrough curve ‘b’ of Fig. 3 was significantly improved, with a breakthrough time $t_b = 1180$ min and a slope at $t_{50\%}$ equal to 0.00331 mg.L⁻¹.mL⁻¹, values being much higher than those measured on curve ‘a’ ($t_b = 730$ min and a slope at $t_{50\%}$ equal to 0.00058 mg.L⁻¹.mL⁻¹).

The column capacity, Q_{total} (mg), for a given inlet concentration (around 10.5 mg of iron per liter) and flow rate ($F = 5$ ml.min⁻¹) is equivalent of the area under the curve of adsorbed Fe(II) concentration versus time (t in min), where C_i and C_e represent the column inlet and effluent Fe(II) concentration, respectively. The column capacity can then be determined from the following equation:

$$Q_{total} = \frac{F}{1000} \int_{t=0}^{t=t_{total}} (C_{ads} dt) \quad \text{with } C_{ads.} = C_i - C_e \quad (2)$$

The volumes of effluent collected at a time t and at the final time of the column experiment (t_{total}) are given by:

$$V_e = F.t \quad \text{and} \quad V_e(\text{final}) = F.t_{total} \quad (3)$$

The total amount of ferrous ion delivered to the column system (m_{total}) is obtained from the equation:

$$m_{total}(\text{mg}) = \frac{C_i \cdot F \cdot t_{Total}}{1000} \quad (4)$$

The equilibrium metal ion uptake, q_{eq} , also known as the column maximum capacity, is given by:

$$q_{eq}(\text{mg/g}) = \frac{Q_{total}}{X} \quad (5)$$

where X is the mass of adsorbent (in gram) packed in the column. As for the removal efficiency Y (%), it was calculated from the equation:

$$Y(\%) = 100 \cdot \frac{Q_{total}}{m_{total}} \quad (6)$$

Column parameters and breakthrough data were reported in Table 1.

Table No. 1: Fixed-bed column parameters and Thomas model data relative to the adsorption of iron(II) in alkali brick.

BREAKTROUGH CURVES	Column parameters and Thomas model results								
	F ml/min	m_{total} mg	X g	Q_{total} mg	Y %	$q_{eq}(\text{Th.})$ mg/g	q_{eq} mg/g	$k_{Th.}$ L/mg/min	R^2
curve (a) in Fig.3	5	141.37	10.09	67.79	47.95	6.0565	6.7185	0.6069	0.9964
curve (b) in Fig.3	5	122.64	10.89	81.17	66.19	7.5930	7.4559	0.6849	0.9986

Overall it was shown that, from the column capacity modeling, the alkali brick leached with a $1.5\text{mol.L}^{-1}\text{NaCl}$ solution had a higher capacity for iron(II) removal than that found with the NaCl-unleached brick.

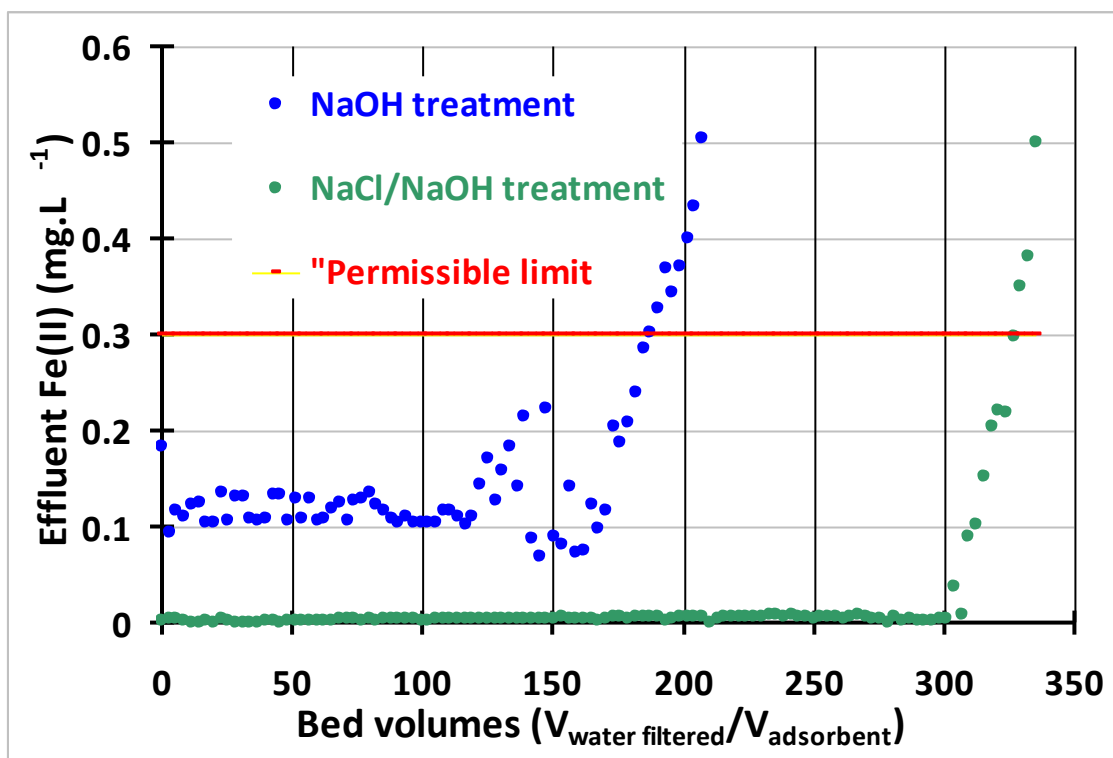


Figure No. 4: Evolution of the quantity of iron(II) adsorbed on alkali-brick pellets in spiked waters as a function of bed volumes. And comparison of the levels of Fe(II) concentrations in treated waters with the permissible limit recommended for iron(II) in drinking water by the World Health Organization (WHO), *i.e.*: 0.3 mg.L⁻¹ [1].

On the other hand, Fe(II) removal ability for alkali-brick pellets without and with a 1.5 mol.L⁻¹ NaCl leaching—which was illustrated in Fig. 4 by the amount of adsorbed Fe(II) *versus* bed volumes— was compared with the permissible limit recommended for iron(II) in drinking water by the World Health Organization (WHO), *i.e.*: 0.3 mg.L⁻¹ [1].

The performed column tests showed clearly a better Fe(II) removal ability for alkali-brick pellets which were previously leached with the NaCl solution than that for alkali-brick pellets not leached (Fig. 4). As can also be seen in this figure, the effluent Fe(II) concentration for the alkali-brick column leached with NaCl exceeded the WHO maximum contaminant level of 0.3 mg.L⁻¹ only after 327 bed volumes of the water had been filtered, corresponding to a volume of about 5.8 liters. Whereas the effluent Fe(II) concentration for the alkali-brick column not leached with NaCl exceeded the WHO maximum contaminant level of 0.3 mg.L⁻¹ [1] when only 190 bed volumes of the water had been filtered, corresponding to a volume of less than 3.4 liters. Furthermore, the effluent Fe(II)

concentration range obtained with ‘NaCl-leached’ alkali brick (from 0.001 to 0.008 mg.L⁻¹) was found to be very much lower than that for NaCl-unleached alkali brick (from 0.069 to 0.223 mg.L⁻¹), and hence, indicating a nearly thorough elimination of iron(II) from polluted water (Fig. 4).

3.4. Fixed-bed adsorption process modeling

In an effort to better explain column dynamics, an adsorption process model was applied to the column system. From continuous flow adsorption experiments, the concentration profile of the liquid and adsorbent phases changes both temporally and spatially [43]. By utilizing breakthrough curves data, design and optimization of packed-bed column operation can be made from a simple mathematical and quantitative modeling approach. Such a model can provide us relevant brick capacity information that would be used for iron(II) removal in the *field* and column regeneration processes. Indeed, knowing when the loaded column must be regenerated is very important in order to optimize at best Fe(II) uptake process and column recovery.

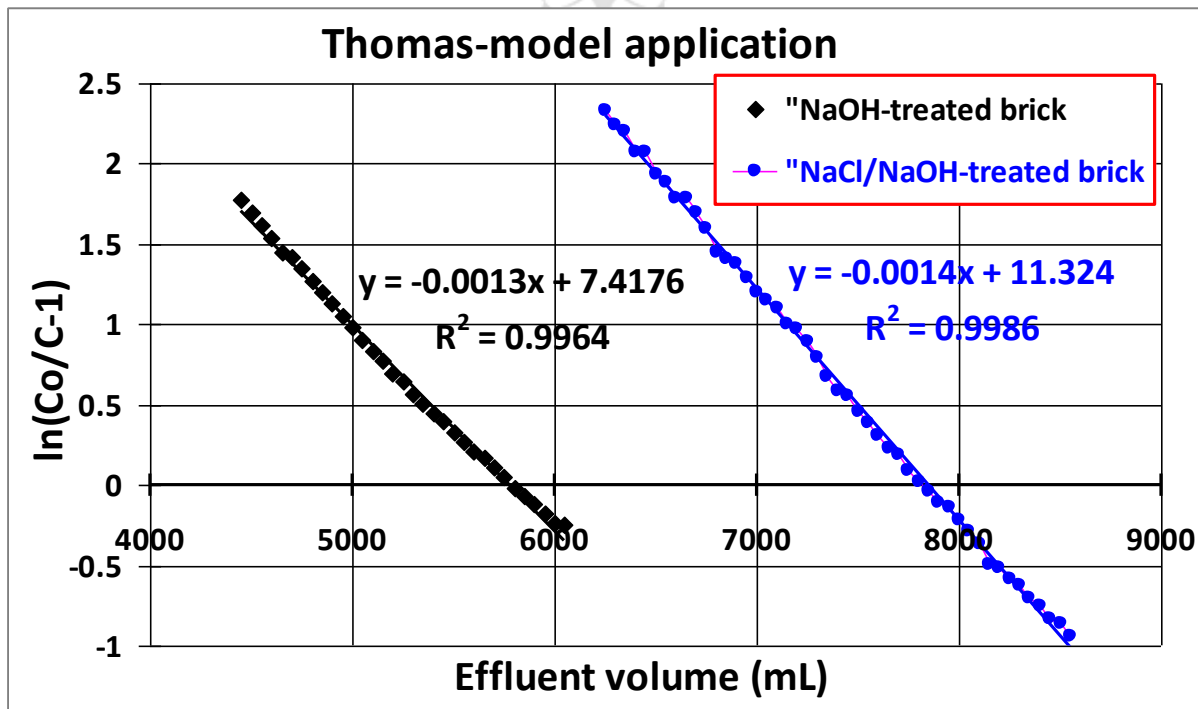


Figure No. 5: Linear fit of Thomas model equation to the breakthrough-curve analysis of the iron(II) adsorption on to alkali-brick pellets.

The Thomas model was applied here to predict breakthrough performance and column capacity constants. The Thomas-model expression can be written as:

$$\frac{C_t}{C_o} = \frac{1}{1 + \exp(k_{Th} / F)(q_{eq(Th.)} \cdot X - C_o \cdot V_{eff.})} \quad (8)$$

where k_{Th} ($\text{mL} \cdot \text{min}^{-1} \cdot \text{mg}^{-1}$) is the Thomas rate constant; $q_{eq(Th.)}$ ($\text{mg} \cdot \text{g}^{-1}$) is the maximum adsorption capacity for iron(II); X (g) is the total mass of the adsorbent loaded in the column; F ($\text{mL} \cdot \text{min}^{-1}$) is the volumetric flow rate; and $V_{eff.}$ (mL) the volume of metal solution passed through the column. The linear form of the Thomas model is given by:

$$\text{Ln}\left(\frac{C_o}{C_t} - 1\right) = \frac{k_{Th} \cdot q_{eq(Th.)} \cdot X}{F} - \frac{k_{Th} \cdot C_o \cdot V_{eff.}}{F} \quad (9)$$

By fitting the experimental data to the model represented in linear form as: $\text{Ln}(C_o/C_t - 1)$ versus $V_{eff.}$ ($V_{eff.}$ as the effluent volume; see Fig. 5), Thomas model constant ($k_{Th.}$) can be calculated from the slope of the plot and the equilibrium capacity ($q_{eq(Th.)}$) can be calculated from the intercept of the plot. Thomas model data are reported in Table 1. The Thomas model's correlation coefficients are high ($R^2 = 0.9964-0.9986$), indicating that the model is able to describe satisfactorily the dynamic behavior of this column system.

3.5. Continuous mode investigation of column for desorption-adsorption

In order to assess the possibility for the reuse of alkali brick after column saturation and recovery of iron(II) ions, the regeneration of the adsorbent was examined in the present work. For that, the same column was packed with 10.1 g of alkali brick pellets ($\Phi \approx 0.7-1.0$ mm). The flow rate was $5 \text{ mL} \cdot \text{min}^{-1}$, and the initial iron(II) concentration was around $10.5 \text{ mg} \cdot \text{L}^{-1}$ in the influent solution. After the column was saturated with Fe^{2+} ions, the desorption of the metal loaded brick pellets was performed with $1.5 \text{ mol} \cdot \text{L}^{-1}$ NaCl, and subsequently, the column pH was increased by passing a $0.01 \text{ mol} \cdot \text{L}^{-1}$ NaOH through the column. As it can be seen in Fig. 3 that the desorbed brick pellets were able to separate Fe(II) ions from the influent up to 3 cycles with a decreasing adsorption percentage of 44.14%, 39.62% and 33.59% after carrying out the first, second and third column regeneration, respectively. The breakthrough times (t_b) were 2000 min, 1400 min and 1175 min in the first, second and third cycles, respectively (Figs. 3c,d,e), revealing a loss of column efficiency. As expected, there was a decreasing trend in the exhaustion time ($t_{exh.}$): 4125 min, 3700 min in the first and

second cycles, respectively. However, the exhaustion time increased at 3950 min in the third cycle. The mechanism of adsorption of iron(II) on zeolitized brick would occur in part according to a diffusion phenomenon through macro-pores and micro-pores toward distinct (sodic) negatively charged sites. In agreement with this, ^{23}Na MAS NMR spectra of alkali brick indicated a highly hydrated state of the sodium in the material, and ^1H MAS NMR spectra revealed distinct water molecules (bound to Na^+ ions) in the α -cages and sodalite (β -) cages of zeolite Na-A [44, 45]. Since alkali brick possesses a broad (meso)pore size distribution, adsorption should remove preferentially hydrated sodium from larger pores like those present in the zeolite Na-A (in α -cages) [44, 45]. Under these conditions, Fe(II) desorption is dependent upon the degree of mobility of Fe^{2+} ions through channels/cavities in the internal structures of brick zeolites. Consequently, after the first column regeneration a part of adsorptive sites remained occupied with (less mobile) Fe^{2+} ions in alkali-brick pores and thereby the subsequent adsorption occurred only on certain type(s) of sites of the material. Indeed, during the column regeneration some adsorbed iron ions were so strongly embedded into specific cavities/channels than these latter prevented adsorbates to be replaced by Na^+ ions (in excess) present in the NaCl leaching solution passing through the column.

Moreover, by performing the 4th regeneration we tried to desorb more Fe^{2+} ions from the Fe(II)-saturated column (after carrying out 3 adsorption-desorption cycles) by treating the material in 'batch' with a $1.5\text{mol.L}^{-1}\text{NaCl}$ solution (as described above) followed by a $0.01\text{mol.L}^{-1}\text{NaOH}$ solution. The fifth regeneration was performed subsequently by passing through the Fe(II)-saturated column a $1.5\text{mol.L}^{-1}\text{NaCl}$ solution (as described above) followed by a more concentrated NaOH solution than that used in the four preceding regenerations ($0.6\text{mol.L}^{-1}\text{NaOH}$ for the fifth regeneration, instead of $0.01\text{mol.L}^{-1}\text{NaOH}$ used for the first, second, third, and fourth regenerations). Column data showed a breakthrough time enhancement after the fourth and fifth regeneration when compared to the breakthrough time obtained after the third regeneration, confirming improved column efficiency in 'batch' and in response to a higher alkaline pre-treatment of the brick (see Table 2).

Table No. 2: Fixed-bed column data obtained for the adsorption of iron(II) on to alkali brick (AB) before and after each desorption-adsorption cycle (five cycles were performed successively in the same adsorbent material).

COLUMN EXPERIMENTS	Fixed-bed column results					
	F ml/min	m _{total} mg	X g	Q _{total} mg	Y %	q _{eq} mg/g
Ads. with NaCl-leached AB	5	141.37	10.09	67.79	47.95	6.72
Ads. after 1st regeneration	5	56.00	10.09	29.92	53.44	2.97
Ads. after 2nd regeneration	5	59.16	10.09	26.86	45.40	2.66
Ads. after 3rd regeneration	5	53.00	10.09	22.77	42.96	2.26
Ads. after 4th regen. (in batch)	5	60.55	10.00	25.49	42.10	2.55
Ads. after 5th regeneration	5	68.00	10.09	31.20	45.88	3.09

AB : alkali brick.

Unfortunately, under high alkaline conditions the degradation of the brick occurred rapidly after repeated NaOH treatments due to the instability of generated zeolites.

4. CONCLUSION

NaOH-treated brick had been successfully used in a continuous column process for the removal of Fe²⁺ ions from iron(II)-spiked water. The experimental data fitted well with the Thomas model. Column regeneration was conducted after iron(II) saturation in order to investigate the reusability of the adsorbent . After three regeneration cycles, the material still showed good removal ability (up to about 34%), and this could be improved by increasing the NaOH concentration in the reagent used for regeneration. Column packed with alkali brick pellets which were previously eluted with a 1.5mol.L⁻¹ NaCl, showed better Fe(II) removal ability than that not eluted. After passing through ‘NaCl eluted’ alkali brick pellets, the effluent iron(II) concentration was found to be much lower (up to 1 µg.L⁻¹) than the permissible limit recommended by the WHO (0.3 mg.L⁻¹), and begun to exceed the “WHO Permissible Limit” level when about 327 bed volumes of the spiked water had been filtered, i.e. corresponding to a volume of about 5.8 liters of safe drinking water. This finding strongly supported the view that NaOH-treated brick after elution with NaCl possessed a high

adsorptive capacity and could then be applicable to treatment of iron(II)-contaminated ground waters in Central African Republic to prevent certain health risks due to elevated levels of iron in water mostly to poor / rural population.

ACKNOWLEDGMENTS

This research was partly funded by the “Agence de l’Eau Artois-Picardie,” and the “City Hall of Villeneuve d’Ascq”. These investigations were undertaken successfully owing to the cooperation between the University of Lille1 (France) and the University of Bangui (Central African Republic). This collaboration (being still under way) and the Grant-in-Aid to Ms. N. Poumaye in for her Doctoral-Thesis preparation have been financially supported by the Embassy of France to Bangui. The authors gratefully thank David Dumoulin (Chemical Engineer) and Christine Grare and V. Alaimo (Chemical Technicians) for helping us usefully in certain delicate chemical and/or analytical/spectroscopic analyses, and Laurence Burylo for having recorded and indexed X-ray diffractograms of our samples.

REFERENCES

1. World Health Organization, Guidelines for Drinking Water Quality, recommendations, Vol. 1, WHO, Geneva, Switzerland, 1984, p. 79.
2. S. Chaturvedi, P.N. Dave, Removal of iron for safe drinking water, *Desalination* 303 (2012) 1-11.
3. N. Khatri, S. Tyagi, D. Rawtani, Recent Strategies for the removal of iron from water: A review, *Journal of Water Process Engineering* 19 (2017) 291-304.
4. G.D. Michalakos, J.M. Nieva, D.V. Vayenas, G. Lyberatos, Removal of iron from potable water using a Trickling filter, *Wat. Res.* 31(5) (1997) 991-996.
5. P. Colvin, V. Filipova, A. Masic, Iron Removal.VVAN01 Decentralized Water and Wastewater Treatment, (2017) www.chemeng.lth.se/vvan01/Arkiv/ExerciseB_Ironremoval.pdf2011
6. Tech Brief: Iron and Manganese Removal, A National Drinking water Clearinghouse Fact Sheet, NINE-September 1998, item #DWBLPE70, 1998, pp. 1-4.
7. R. P. Bailey, T. Bennett and M. M. Benjamin, “Sorption onto and Recovery of Cr(VI) Using Iron Oxide-Coated Sand,” *Water Science & Technology*, Vol. 26, No. 5-6, 1992, pp. 1239-1244.
8. S. Khaodhiar, M. F. Azizian, K. Osathaphan and P. E. Nelson, “Copper, Chromium and Arsenic Adsorption and Equilibrium Modeling in an Iron-Oxide-Coated Sand, Background Electrolyte System,” *Water, Air, Soil Pollution*, Vol. 119, No. 1-4, 2000, pp. 105-120. doi:10.1023/A:1005109325539
9. A. Joshi and M. Chaudhuri, “Removal of Arsenic from Ground Water by Iron-Oxide-Coated Sand,” *Journal of Environmental Engineering* 122(8) (1996) 769-800. doi:10.1061/(ASCE)0733-9372(1996)122:8(769)
10. M. M. Benjamin, R. S. Sletten, R. P. Bailey and T. Bennett, “Sorption and Filtration of Metals Using Iron-Oxide-Coated Sand,” *Water Research* 30(11) (1996) 2609-2620. doi:10.1016/S0043-1354(96)00161-3
11. M. M. Ahammed and K. Davra, “Performance Evaluation of Biosand Filter Modified with Iron Oxide-Coated Sand for Household Treatment of Drinking Water,” *Desalination* 276(1-3) (2011) 287-293. doi:10.1016/j.desal.2011.03.065
12. B. Rusch, K. Hanna and B. Humbert, “Coating of Quartz Silica with Iron Oxides: Characterization and Surface Reactivity of Iron Coating Phases,” *Colloids and Surfaces A: Physicochemical and Engineering Aspects* 353(2-3) (2010) 172-180. doi:10.1016/j.colsurfa.2009.11.009

13. M. M. Ahammed and V. Meera, "Metal Oxide/Hydroxide-Coated Dual-Media Filter for Simultaneous Removal of Bacteria and Heavy Metals from Natural Waters," *Journal of Hazardous Materials* 181(1-3) (2010) 788-793. doi:10.1016/j.jhazmat.2010.05.082
14. C.-S. Jeon, K. Back, J.-K. Park, Y.-K. Oh and S.-D. Lee, "Adsorption Characteristics of As(V) on Iron-Coated Zeolite," *Journal of Hazardous Materials* 163(2-3) (2009) 804-808. doi:10.1016/j.jhazmat.2008.07.052
15. R. Han, L. Zou, X. Hao, Y. Xu, F. Xu, Y. Li and Y. Wang, "Characterization and Properties of Iron-Oxide-Coated Zeolite as Adsorbent for Removal of Copper(II) from Solution in Fixed Bed Column," *Chemical Engineering Journal* 149(1-3) (2009) 123-139. doi:10.1016/j.cej.2008.10.015
16. E. Eren and H. Gumus, "Characterization of the Structural Properties and Pb(II) Adsorption Behavior of Iron Oxide Coated Sepiolite," *Desalination* 273(2-3) (2011) 276-284. doi:10.1016/j.desal.2011.01.004
17. Dehou, S.C., Mabingui, J., Lesven, L., Wartel, M., Boughriet, A. Improvement of Fe(II)-adsorption capacity of FeOOH-coated brick in solutions, and kinetics aspects. *J. Water Resour. Protection* 4 (2012) 464-473.
18. Allahdin, O., Dehou, S.C., Wartel, M., Recourt, P., Trentesaux, M., Mabingui, J., Boughriet, A. Performance of FeOOH-brick based composite for Fe(II) removal from water in fixed bed column and mechanistic aspects. *Chem. Eng. Res. and Design* 91 (2013) 2732-2742.
19. Allahdin, O., Wartel, M., Recourt, P., Revel, B., Ouddane, B., Billon, G., Mabingui, J., Boughriet, A. Adsorption capacity of iron oxyhydroxide-coated brick for cationic metals and nature of ion surface interactions. *Applied Clay Science* 90 (2014) 141-149.
20. Allahdin, O., Wartel, M., Mabingui, J., A. Boughriet, A. Kinetics of divalent Metals (Cd^{2+} , Cu^{2+} , Pb^{2+} , Zn^{2+}) adsorption onto a modified brick. *Am. Chem. Sci. J.* 4(5) (2014) 687-705.
21. Allahdin, O., Wartel, M., Mabingui, J., Boughriet, A. Implication of electrostatic forces on the adsorption capacity of a modified brick for the removal of divalent cations from water. *Am. J. Anal. Chem.* 6 (2015) 11-25.
22. S. C. Dehou, M. Wartel, P. Recourt, B. Revel, J. Mabingui, A. Montiel and A. Boughriet. Physicochemical, crystalline, and morphological characteristics of bricks Used for ground waters purification in Bangui region (Central African Republic). *Applied Clay Science* 59-60 (2012) 69-75. doi:10.1016/j.clay.2012.02.009
23. W. Stumm, J.J. Morgan. *Aquatic Chemistry: Chemical Equilibria and Rates in Natural Waters*. Third Edition. Environmental Science and Technology. John Wiley & Sons, INC., New York. 1996; p. 461.
24. J. Hartmann, F. Bräulke, U. Sinzig, G. Wulf, J.H. Maas, F. Konietzschke, D. Haase, Iron overload impairs proliferation of erythroid progenitors cells (BFU-E) from patients with myelodysplastic syndromes, *Leuk. Res.* 37 (2013) 327-332.
25. X. Chai, D. Li, X. Cao, Y. Zhang, J. Mu, W. Lu, X. Xiao, C. Li, J. Meng, J. Chen, Q. Li, J. Wang, A. Meng, M. Zhao, ROS-mediated iron overload injures the hematopoiesis of bone marrow by damaging hematopoietic stem/progenitor cells in mice, *Sci. Rep.* 5 (2015) 10181.
26. Y.Y. Jang, S.J. Sharkis, A low level of reactive oxygen species selects for primitive hematopoietic stem cells that may reside in the low-oxygenic niche. *Blood* 110 (2007) 3056-3063.
27. L. Shao, H. Li, S.K. Pazhanisamy, A. Meng, Y. Wang, D. Zhou. Reactive oxygen species and hematopoietic stem cell senescence. *Int. J. Hematol.* 94 (2011) 24-32.
28. C. Fripiat, J. Dewelle, J. Remacle, O. Toussaint. Signal transduction in H_2O_2 induced senescence - like phenotype in human diploid fibroblasts, *Free Radic. Biol. Med.* 33 (2002) 1334-1346.
29. E. Prus, E. Fibach, Effect of iron chelators on labile iron and oxidative status of thalassaemic erythroid cells, *Acta Haematol.* 123 (2010) 14-20.
30. World Health Organization (WHO). *Iron in Drinking-water*. In: WHO Guidelines for drinking-water quality, 2nd ed. Vol. 2. Health criteria and other supporting information. World Health Organization, Geneva, 1996.
31. USEPA, 2011. *Exposure Factors Handbook*. United States Environmental Protection Agency, Washington, DC (EPA/600/R-09/052F).
32. A. Rasool, A. Farooqi, T. Xiao, S. Masood, M. Aqeel Kamran, S. bibi. Elevated levels of arsenic and trace metals in drinking water of Tehsil Mailsi, Punjab, Pakistan. *Journal of Geochemical Exploration* 169 (2016) 89-99. And references therein.
33. M.M.J. Treacy, J.B. Higgins, *Collection of Simulated XRD Powder Patterns for Zeolites* (4th revised Edition), Elsevier, New York, 2001, pp. 174-175 and 212-215.

34. M.K. Seliem, S. Kormarneni, Equilibrium and kinetic studies for dissociation of iron from aqueous solution by synthetic Na-A zeolites: Statistical modelling and optimization. *Microporous and Mesoporous Materials* 228 (2016) 266-274.
35. S. Tontisirin, Synthesis and characterization of co-crystalline zeolite composite of LSX/A. *Microporous and Mesoporous Materials* 239 (2017) 123-129.
36. M. Sathupunya, E. Glari, S. Wongkasemjit, ANA and GIS zeolite synthesis directly from alumatrane and silatrane by sol-gel process and microwave technique. *J. Eur. Ceram. Soc.* 22 (2002) 2305-2314.
37. H.-L. Zubowa, H. Kosslick, D. Müller, M. Richter, L. Wilde, R. Fricke. Crystallization of phase-pure zeolite NaP from MCM-22-type gel compositions under microwave radiation. *Microporous and Mesoporous Materials* 109 (2008) 542–548.
38. S. Khabuanchalad, P. Khemthong, S. Prayoonpokarach, J. Wittayakun. Transformation of zeolite NaY synthesized from rice husk silica to NaP during hydrothermal synthesis. *Suranaree J. Sc. Technol.* 15 (2008) 225-231.
39. J. Behin, H. Kazemian, S. Rohani. Sonochemical synthesis of zeolite NaP from clinoptilolite. *Ultrasonics Sonochemistry* 28 (2016) 400-408.
40. D. Kratochvil, B. Volesky. Advances in the biosorption of heavy metals. *Trends Biotechnol.* 16(7) (1998) 291-300.
41. Z. Aksu, F. Gönen. Biosorption of phenol by immobilized activated sludge in a continuous packed bed: prediction of breakthrough curves. *Process Biochem.* 39(5) (2004) 599-613.
42. S. Armirmia, M.B. Ray, A. Margaritis. Copper ion removal by *Acer saccharum* leaves in a regenerable continuous-flow column. *Chem. Eng. J.* 287 (2016) 755-764.
43. A. Abdolali, H.H. Ngo, W. Guo, J.L. Zhou, J. Zhang, S. Liang, S.W. Chang, D.D. Nguyen, Y. Liu. Application of a breakthrough biosorbent for removing heavy metals from synthetic and real wastewaters in a lab-scale continuous fixed-bed column. *Bioresour. Technol.* 229 (2017) 78-87.
44. S. Greiser, P. Sturm, G. J.G. Gluth, M. Hunger, C. Jäger, Differentiation of the solid-state NMR signals of gel, zeolite phases and water species in geopolymer-zeolite composites. *Ceramics International* 43 (2017) 2202-2208.
45. N. Poumaye, O. Allahdin, G. Tricot, B. Revel, G. Billon, P. Recourt, M. Wartel, A. Boughriet, MAS NMR investigations on a metakaolinite-rich brick after zeolitization by alkaline treatments, *Microporous and Mesoporous Materials* 277 (2019) 1-9.